

# Mitigating Perspective Distortion-induced Shape Ambiguity in Image Crops

Aditya Prakash   Arjun Gupta   Saurabh Gupta  
University of Illinois Urbana-Champaign  
<https://bit.ly/AmbiguityEnc>

## Abstract

Objects undergo varying amounts of perspective distortion as they move across a camera’s field of view. Models for predicting 3D from a single image often work with crops around the object of interest and ignore the location of the object in the camera’s field of view. We note that ignoring this location information further exaggerates the inherent ambiguity in making 3D inferences from 2D images and can prevent models from even fitting to the training data. To mitigate this ambiguity, we propose *Intrinsics-Aware Positional Encoding (KPE)*, which incorporates information about the location of crops in the image and camera intrinsics. Experiments on three popular 3D-from-a-single-image benchmarks: depth prediction on NYU, 3D object detection on KITTI & nuScenes, and predicting 3D shapes of articulated objects on ARCTIC, show the benefits of KPE.

## 1. Introduction

Making metric predictions from a single image suffers from scale-depth ambiguity. Even when the camera intrinsics are known, it is impossible to disambiguate if Circle A shown in Fig. 1 has a radius of 0.485 cm (say) & is 2 cm away (say) or a radius of 4.85 cm and 20 cm away. Familiar size, or knowledge of the size of a reference object in the image, is a useful cue for resolving this ambiguity [10, 19].

The scale-depth ambiguity is a well-known and fundamental ambiguity. What we describe next is a subtle different ambiguity that occurs when we consider object crops from images for feeding into a neural network. Let’s assume that we are using size familiarity to resolve scale-depth ambiguity, *i.e.* assume that the circles always have a radius of 0.485 cm. Given this information, it should be possible to infer how far they are in the image. This can be readily derived using similar triangles and the *location of the circle’s image in the visual field*. In fact, this principle goes back many centuries and was known to Da Vinci [36].

However, if we consider crops around the object, say those output by an object detector, and try making a prediction for the circle’s distance based on the appearance of the

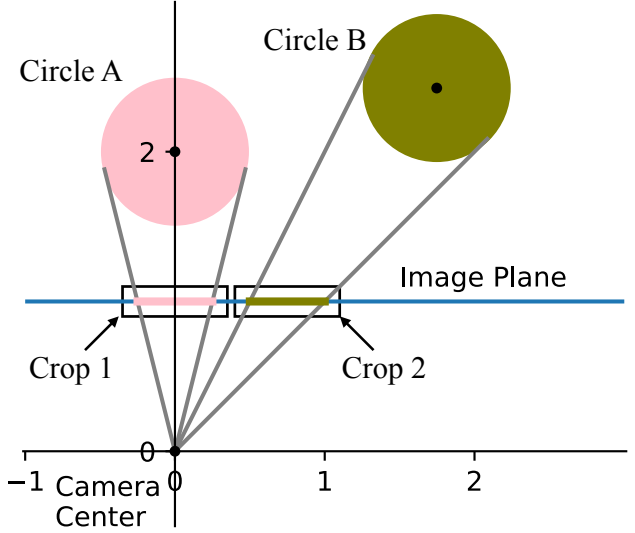


Figure 1. **Perspective Distortion-induced Shape Ambiguity.** Consider two circles of the same size undergoing perspective projection under a pinhole camera. Even though they are at different distances from the camera, they appear to be the same size in the image due to perspective distortion. A model (e.g. a neural network) that predicts the distances of these circles from the camera based purely on the appearance of the image crops, *without taking into account their location in the camera’s field of view*, will fail at this task. We call this the *Perspective Distortion-induced Shape Ambiguity in Image Crops* or *PSAC*. In this work, we propose an encoding to incorporate the crop location in the camera’s field of view as input and show its effectiveness on metric depth prediction, 3D object detection & 3D pose estimation of articulated objects (Sec. 5).

crop, this can prove to be quite difficult. Fig. 1 shows fixed sized center crops around the center of the circle’s image. It turns out, just looking at the crops while ignoring the location of the crop, it is no longer possible to predict the distance of the circle from the camera! A 0.5 cm wide image could correspond to Circle A that is 2 cm away directly in front of the camera, or Circle B that is further away (2.43 cm away) but off to the side. This simple example only exposed global pose error, but our detailed case study in Sec. 3 reveals that this ambiguity exists both in global pose and root-relative

3D shape. We call this *Perspective Distortion-induced Shape Ambiguity in Image Crops or PSAC*.

To mitigate this ambiguity, we propose an intrinsics-aware positional encoding (KPE) that incorporates the location of the crop in the camera’s field of view (Fig. 4). This allows the network to specialize its interpretation of 3D geometry based on the location in the image. We show results on three popular 3D-from-single-image benchmarks: articulated object pose estimation on ARCTIC [12], pixel-wise metric depth predictions on NYUD2 [31] and 3D object detection from monocular images on KITTI [13] and nuScenes [7]. Across these three real world benchmarks and a diagnostic setting, we find this additional information to improve metrics.

We acknowledge that similar encodings have been used in literature [11, 15]. However, their use was motivated by the need to train models across different cameras. Our contribution is to identify perspective distortion-induced shape ambiguity in image crops, even with a single camera, and show the effectiveness of encoding the location of the crop in the camera’s field of view to mitigate this ambiguity.

## 2. Related Work

**Ambiguity in 3D from a single image:** Scale-depth ambiguity is well known and is commonly dealt with by only evaluating 3D predictions up to a scale [29] or after a rigid alignment with the ground truth [21]. Where metric 3D predictions are needed, training is either done using domain specific knowledge [4], camera intrinsics as input [6] or information from predicted camera parameters [20, 23]. Notably, due to this ambiguity, models can not trivially be trained with scale and crop augmentations unless some adjustments are made [6, 9]. Ambiguity induced due to crops (the focus of our work) has not been analyzed in literature to the best of our knowledge. Note that this ambiguity is an artifact of *planar* perspective projection in images and doesn’t exist in spherical perspective projection. The differences and relationship between planar and spherical perspective have been used to simplify analysis, *e.g.* [26].

**Geometric embeddings:** Past works have considered the use of different encodings, based on pixel locations [8, 25], camera intrinsics [11] or extrinsics [37], as input to networks to improve performance. Liu *et al.* [25] show that preserving spatial location of the pixels helps in generative modelling, object detection, and reinforcement learning. Positional encodings, *e.g.* learned [8], relative [33], or rotational [32], are also commonly used in training transformer [35]-based models. Recent works [11, 15] have also studied the effectiveness of pixel-level encodings in multi-dataset setting (with varying cameras) on depth estimation tasks. Researchers have also considered canonicalizing the inputs (captured with different cameras) to a common camera intrinsics [1, 6] to indirectly provide camera information. [14, 27, 37] employ

this idea in multi-view settings. Yifan *et al.* [37] used such encodings to inject geometric inductive biases (*e.g.* the epipolar geometry constraint) into a general perception model for multi-view stereo. Guizilini *et al.* [14] extend this further and use per-pixel embeddings to capture the image coordinate and camera intrinsics & extrinsics for multi-view depth estimation. Miyato *et al.* [27] propose a geometry-aware attention mechanism to encode the geometric structure of tokens in transformers for novel view synthesis tasks.

Our use of the location of the crop in the camera’s field of view as an additional input to neural networks is motivated by these past works. Orthogonal to these works, our contribution is to demonstrate the effectiveness of this encoding in mitigating the perspective distortion-induced shape ambiguity in image crops.

## 3. Parallelepipeds Case Study

We first analyze simple parallelepipeds to intuitively understand the perspective distortion-induced ambiguity in image crops and the effectiveness of the crop location in the camera’s field of view to mitigate this ambiguity. It is important to note that this ambiguity does not always exist. If the shape and size of the object are perfectly known (say we know that it is a front-facing cube), then the location of the cube in the visual field can itself be deduced from an image crop.

However, if the geometry of the object is also unknown, then it may no longer be possible to disentangle shape & pose from a given image crop. Consider the family of 3D shapes with a square face (of width 0.2m lying in XY plane) that is extruded along an arbitrary direction, *i.e.* parallelepipeds with at least one face being a square. Fig. 2 (a.2 top row) shows different parallelepipeds when placed directly in front of the camera (*i.e.* from one consistent viewing angle across the row). Note that the parallelepipeds here do not extend purely in the Z-direction (except for the leftmost reference in green box), but can extend at an oblique angle. Fig. 2 (a.2 bottom row) shows these same parallelepipeds when placed at different locations in the visual field. These locations were mined separately for each so as to maximize the visual similarity to the leftmost reference parallelepiped. As evident, even though the parallelepipeds across the row have different shapes, they all look the same in the 2D image (with a sub-pixel reprojection error), albeit for their 2D locations.

This ambiguity only exists if we only look at the image crops locally without factoring in the absolute 2D location of the crop. Let’s treat the parallelepiped in the first column (a cuboid) as reference. Fig. 2 (a.1) plots the root relative 3D shape error as a function of the root relative 2D keypoint error of different parallelepipeds w.r.t. the reference cuboid. For root relative error, we compute the keypoint error *after* the centers of the parallelepipeds have been aligned. Points are color coded based on the 2D distance of the image crops from the cuboid crop (blue means image crops are closer,

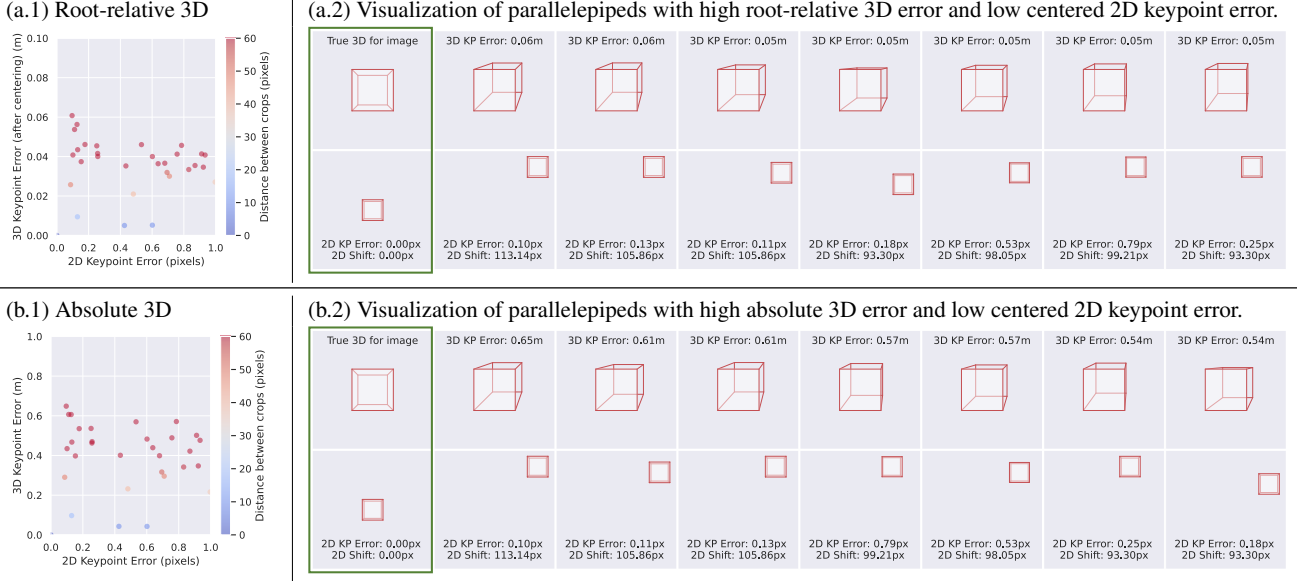


Figure 2. **Parallelepipeds visualization.** Figure (a.1) plots the root relative 3D keypoint error vs. 2D keypoint error of different parallelepipeds placed at different locations in the camera’s field of view w.r.t. a reference cuboid shown in the green box in (a.2). Points are color coded with the distance between the parallelepipeds crops. As we let crops go farther away (the red points), we start finding parallelepipeds that have very different 3D shape but happen to project such that their 2D keypoints look the same as the reference cuboid. Figure (a.2) shows these 3D parallelepipeds in the top row and their renderings in the bottom row. The 1<sup>st</sup> figure in the green box is the reference w.r.t. which we measure 2D and 3D keypoint errors. Figures (b.1) and (b.2) present analogous plots where we measure absolute 3D error (rather than root-relative 3D error).

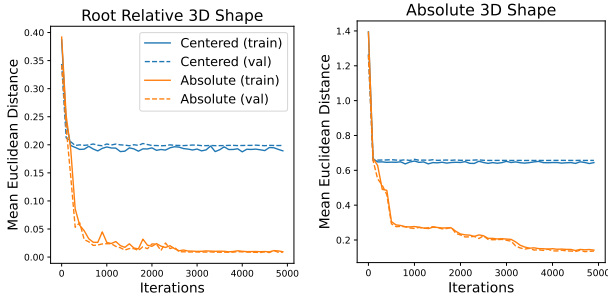


Figure 3. Predicting root relative (left) or absolute (right) 3D shape from 2D image crops fails in the absence of information about the location of the crop in camera’s field of view. Training loss saturates at a high value because of the inherent ambiguity. Adding in information about the location of the crop in camera’s field of view alleviates this ambiguity, leading the network to much better metrics for both root-relative and absolute 3D prediction.

red means they are farther away). If we limit reasoning to only close-by crops, *i.e.* the blue points, low 2D keypoint error implies low 3D shape error. However, if we look at the farther away points (the red points), image with a low relative 2D keypoint error can actually have a high 3D shape error. This is the inherent ambiguity: even if two shapes appear similar visually, their 3D shapes may be vastly

different. Fig. 2 (b.1) and (b.2) present analogous plots where we measure absolute 3D error instead of root-relative error.

Let’s see what happens when we train neural networks to predict 3D shape from the 2D keypoints. Given the 2D coordinates for the 8 corners, the goal is to predict the root-relative (or absolute) 3D location of the 8 corners. We consider two variants. First, we center the eight 2D corners by subtracting their mean to get centered crops. Next, we retain the absolute value of the 2D coordinates. We train a 6-layer MLP with these two inputs. Fig. 3 shows the training and validation plots for predicting root relative and absolute 3D coordinates for the 8 corners. As expected the first version that only uses the crops converges to a higher error even on the training set as it is impossible to infer the 3D shape from centered 2D corners due to the ambiguity. The second version that has access to the absolute coordinates does not suffer from this ambiguity and is able to successfully estimate the 3D shape on both training and validation data.

#### 4. Intrinsic-Aware Positional Encoding (KPE)

We mitigate the ambiguity induced by perspective distortion (Fig. 1) through design of encodings that capture the location of the crop in the camera’s field of view, referred to as Intrinsic-Aware Positional Encodings (KPE). Specifically, let’s denote the principal point for the original image by

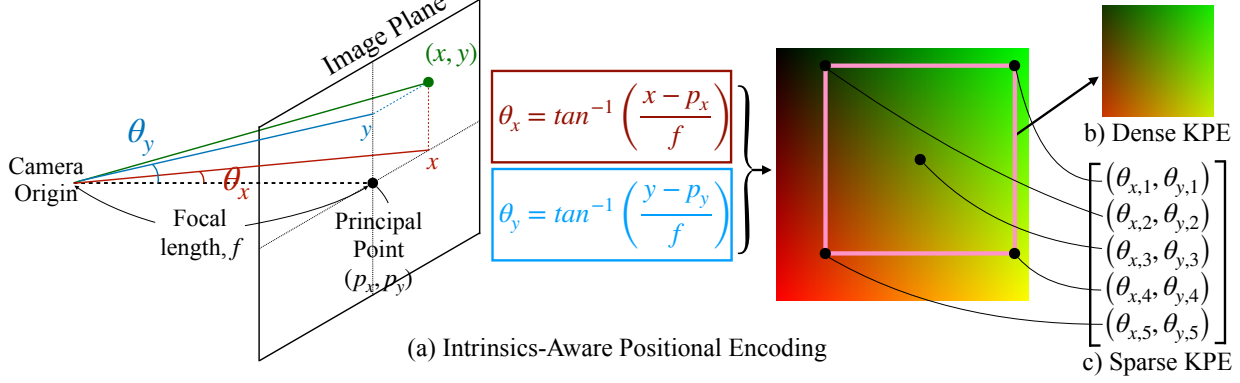


Figure 4. **Intrinsic-Aware Positional Encodings (KPE).** (a) For each pixel in the image, we compute its position in the camera’s field of view ( $\theta_x$  and  $\theta_y$ ), or the angular distance that the pixel makes with respect to the principal point and the camera origin (as shown on the left). Note that both  $\theta_x$  and  $\theta_y$  are sensitive to the camera intrinsic parameters. (b) For a dense prediction task, we make use of a dense prediction encoding which contains the positional encoding for each pixel in the region of interest. (c) For other tasks, we simply represent the positions of the corners of the relevant region of interest in addition to the center point. The positional encoding can be passed into the network at the input level or concatenated to some intermediate representation, this design choice is made separately for each task.

$(p_x, p_y)$  and focal length by  $(f_x, f_y)$ . For any pixel  $(x, y)$ , we can describe its position in the camera’s field of view via  $\theta_x = \tan^{-1} \left( \frac{x - p_x}{f_x} \right)$  and  $\theta_y = \tan^{-1} \left( \frac{y - p_y}{f_y} \right)$ . Our proposal is to retain this information for pixels when images are cropped or resized for feeding into neural networks.

KPE can be used in different ways (Fig. 4). For a dense prediction task, *e.g.* depth estimation, we can concatenate this encoding in a dense manner to an intermediate feature map (or also to input pixels). For tasks that involve summarizing the geometric properties for objects, *e.g.* predicting its 3D bounding box or 3D pose, we consider a sparse variant, which encodes the center and corners of the relevant region of interest. We use both these variants in our experiments.

## 5. Experiments

We consider 3 challenging settings, involving the prediction of 3D geometric attributes from a single image, to show the effectiveness of KPE: 3D pose estimation of articulated objects in contact, dense depth prediction and 3D object detection. These tasks constitute both sparse and dense prediction of 3D attributes. Since our goal is to show the utility of KPE (not to achieve state-of-the-art results) we select some representative models from recent works on each of these tasks and incorporate KPE into their architectures.

### 5.1. 3D Pose of Articulated Objects in Contact

**Task:** Given an egocentric image showing an articulated object in interaction, the goal is to estimate the 3D pose of the object in contact. This setting often involves occlusions induced by hands which makes it quite challenging. In such cases, additional cues about the spatial location or perspective distortion may provide a useful signal for pose

prediction. Specifically, the 3D pose is represented using rotation in the camera coordinate frame, the translation of the root of the object with respect to the camera center and the angle of articulation between the bottom and top components of the articulated object. The object mesh is assumed to be available. We also consider contact estimation and 4D motion reconstruction to show the versatility of KPE.

**Method:** We adopt the single-image ArcticNet-SF [12] architecture released with the ARCTIC benchmark [12]. The network takes a single image as input, which is processed by a ResNet50 [17] backbone to get a feature map of resolution  $7 \times 7 \times 2048$ . These features are then average pooled and passed to a decoder to predict the 7-dimensional pose, consisting of rotation, translation & articulated angle of the object. The decoder iteratively predicts these entities using a HMR [22]-style architecture. For iterative prediction, the rotation and translation are initialized as a 0-vector whereas the initial articulation angle is predicted using the global features from the convolutional backbone. The network outputs rotation in axis-angle format and uses the weak perspective camera model to estimate the translation [5, 22, 24, 38]. The entire network is trained end-to-end using an L2 loss between the predictions and the ground truth for 7-dimensional pose, 3D keypoints and 2D projection of 3D keypoints.

**Modifications:** We modify the architecture to also take crops around the object as input, which are processed by a ResNet50 backbone [18]. Since our network requires object crops, we also train a bounding box predictor model by fine-tuning MaskRCNN [18] on the ARCTIC training set using the ground truth bounding box computed from the 2D projections of 3D object keypoints. This is required to evaluate our model on the online leaderboard for which



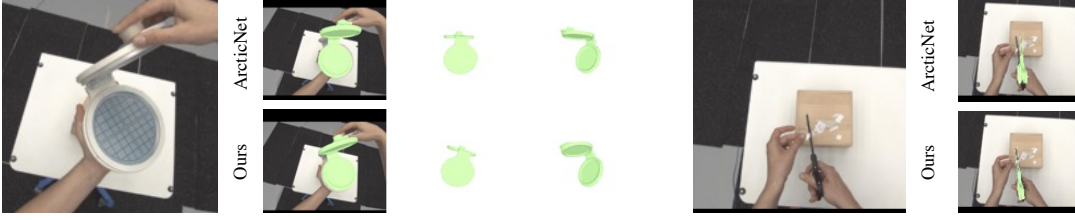


Figure 5. **3D pose visualizations on ARCTIC.** Our proposed modification of intrinsics-aware positional encoding (KPE) improves over the ArcticNet-SF [12] model by predicting better 3D poses in interaction scenarios (note the difference in the articulation angle and global pose). For each image, we show the projection of the object mesh with the predicted pose on the image and from 2 different camera views.

	Method	Object		Contact		Motion	
		AAE( $^{\circ}$ ) $\downarrow$	Success(%) $\uparrow$	CDev <sub>ho</sub> (mm) $\downarrow$	MRRPE <sub>ro</sub> (mm) $\downarrow$	MDev <sub>ho</sub> (mm) $\downarrow$	Acc(m/s <sup>2</sup> ) $\downarrow$
val split	ArcticNet-SF [12]	8.0	59.0	44.1	36.8	11.8	11.3
	+ KPE sparse	<b>5.9</b>	<b>71.5</b>	<b>39.4</b>	<b>29.7</b>	<b>9.3</b>	<b>8.7</b>
test split	ArcticNet-SF [12]	6.4	53.9	44.7	36.2	11.8	9.1
	+ KPE sparse	<b>5.2</b>	<b>64.1</b>	<b>36.5</b>	<b>28.3</b>	<b>10.5</b>	<b>7.6</b>

Table 1. **3D pose estimation of articulated objects in contact.** We compare with ArcticNet-SF on multiple geometric tasks: 3D pose, contact and 4D motion estimation for articulated objects on ARCTIC. Our intrinsics-aware positional encoding leads to significant improvements across all metrics (See Sec. 5.1 for details). We use the sparse variant of KPE for these experiments.

ground truth is not available. For contact prediction, we use the hand pose from the default ArcticNet-SF decoder.

**Incorporating KPE:** As described in Sec. 4, we explore both sparse (captures only the center and corner pixels of the object crop) and dense (encode each pixel in the crop). We consider 3 choices for where to add KPE in the model: (1) concatenate with the input, (2) process the encoding with a MLP & add with the average pooled global features, (3) interpolate the encoding to  $7 \times 7$  resolution & concatenate with  $7 \times 7 \times 2048$  feature map from the last convolutional layer of ResNet50. This concatenated feature is then processed by three convolutional layers and flattened to 2048 dimensions before being passed to the decoder. We do not use batchnorm in these 3 convolutional layers.

**Dataset:** ARCTIC [12] is a recent dataset consisting of hands interacting with articulated objects in a free-form manner. We select this dataset since it has a large range of dexterous interactions compared to existing datasets [16, 34]. There are 2 settings in the dataset: 1.5M frames from 8 allocentric views & 200K frames from 1 egocentric view. We show results in egocentric setting since the perspective distortion is more prominent due to objects being closer to the camera. The released dataset does not contain ground truth for test set, which is evaluated separately on the online leaderboard. We compare with ArcticNet-SF in this setting.

**Metrics:** We follow the evaluation protocol of the ARCTIC benchmark [12] and report the following metrics:

- **AAE:** Average Absolute Error between the ground truth

degree of articulation and the prediction.

- **Success:** percentage of predicted object vertices with L2 error  $< 5\%$  of the diameter of the object.
- **CDev:** Contact Deviation is average distance between the predicted in-contact hand-object vertices and ground truth
- **MRRPE:** Mean Relative-Root Position Error between the predicted root keypoint location and the ground truth.
- **MDev:** Between consecutive frames, Motion Deviation measures the disagreement in the direction of the movement of in-contact hand-object vertices.
- **ACC:** Acceleration error is the difference in the predicted acceleration of the vertices and the ground truth.

**Results:** Adding KPE to ArcticNet-SF leads to consistent improvements across the 3D pose, contact and 4D motion estimation metrics (Tab. 1). We also ablate the sparse and dense variants of our encoding in Tab. 4. The dense variant is worse than the sparse variant, which could be due to the task requiring sparse predictions and the network getting confused by the spatial information about distractors around the object. In terms of design choices, we find that inserting KPE at the  $7 \times 7$  feature map level works better than adding it at the input or at the global feature level.

For each image, we visualize (in Fig. 5) the projection of the object mesh (assumed to be available) in the image using the predicted 7-dimensional pose (global rotation, camera translation & articulation angle) along with renderings of the shape from two additional views. From the visualizations, we observe that KPE leads to better angle of articulation and global rotation than ArcticNet-SF.

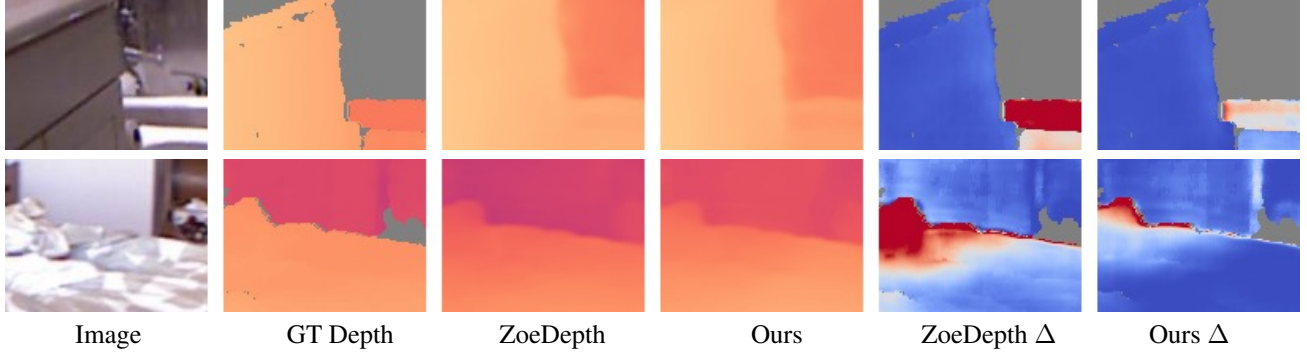


Figure 6. **Depth visualizations on NYU.** We compare the depth predicted by adding KPE encoding to ZoeDepth [4] with the base ZoeDepth model, on  $96 \times 128$  input crops. We show the depth predictions along with the squared error  $\Delta$  w.r.t. to ground truth depth (ranging from dark blue: low to dark red: high, invalid regions are indicated as grey). Our model predicts better depth as evident by lower  $\Delta$  (lower intensity red areas). Gains are more prominent in this low resolution setting compared to  $384 \times 512$  setting (Fig. in supplementary).

## 5.2. Dense Metric Depth Prediction

**Task:** Metric depth prediction from a single image is ill-posed due to depth-scale ambiguity [9], so several works [28, 29] focus on predicting depth up to scale. This could be mitigated to some extent by using domain knowledge about specific datasets, as in ZoeDepth [4]. However, this gets worse in the presence of augmentations, *e.g.* cropping and scaling [39], due to which these augmentations are excluded during training. Here, we investigate whether additional cues from KPE about the crop location & camera intrinsics could help to improve metric depth estimation in the presence of cropping and scaling augmentations.

**Method:** We adopt the architecture of ZoeDepth [4]. It consists of a transformer-based MiDaS [29] backbone to estimate relative depth, which is passed to a domain specific decoder along with multi-scale image features from the backbone, to predict the metric depth for each dataset separately. The model uses a discretized representation of 3D space (into a volumetric grid, referred to as bins) to first output coarse depth (represented as the center of the bin), which is then refined by an MLP in subsequent layers (referred to as the MetricBins [4] module). The model is trained using the scale-invariant log loss (similar to [3]) with  $384 \times 512$  images without any cropping and scaling augmentations during training. There are two variants of the model: trained from scratch and initialized from a MiDaS model pre-trained on 12 datasets (also on  $384 \times 512$  images).

**Modifications:** We use cropping & scaling augmentations during training and operate at 2 sizes:  $96 \times 128$  &  $384 \times 512$ . We do not change the architecture or loss function.

**Incorporating KPE:** We explore two design choices to add KPE: (1) with the relative depth &  $12 \times 16 \times 256$  image features predicted by the MiDaS model, before passing it to

Method	REL ↓	RMSE ↓	$\log_{10}$ ↓
$96 \times 128$ crops			
ZoeD-X-N	0.182	0.538	0.078
ZoeD-X-N + KPE dense	<b>0.175</b>	<b>0.516</b>	<b>0.074</b>
ZoeD-M12-N	0.187	0.536	0.079
ZoeD-M12-N + KPE dense	<b>0.182</b>	<b>0.516</b>	<b>0.074</b>
$384 \times 512$ crops			
ZoeD-X-N	0.090	0.353	<b>0.039</b>
ZoeD-X-N + KPE dense	<b>0.089</b>	<b>0.350</b>	<b>0.039</b>
ZoeD-M12-N	0.084	0.337	0.037
ZoeD-M12-N + KPE dense	<b>0.082</b>	<b>0.329</b>	<b>0.036</b>

Table 2. **Dense metric depth prediction on NYU.** We test the effectiveness of adding KPE to models trained at different resolutions:  $96 \times 128$  input with cropping and scaling augmentation,  $384 \times 512$  input. We observe larger gains in the former, indicating that our encoding helps with cropping and scaling augmentations. The gains are less evident in the  $384 \times 512$  setting due to strong initialization from MiDaS model pretrained on 12 different datasets. We use the dense variant of KPE here.

the MetricBins module, (2) with the downsampled  $24 \times 32 \times 1024$  feature map before being processed by the BeiT [2] module in MiDaS. We interpolate KPE to a resolution of  $12 \times 16$  for the former and  $24 \times 32$  for the latter, in case of the dense variant. For the sparse variant, we broadcast it to the required resolution.

**Dataset:** We use NYU Depth v2 [31], a popular indoor scene dataset, captured over 450+ unique scenes. We consider the same splits as [4], *i.e.* 23K images for training, 654 images for testing and compare with ZoeDepth [4]. Similar to the training, we evaluate the models at  $96 \times 128$  and  $384 \times 512$ .

**Metrics:** Following [4], we compute 3 metrics between the predicted metric depth ( $\hat{d}_i$ ) and the ground truth ( $d_i$ ): (1) **REL**: absolute relative error,  $\frac{1}{M} \sum_{i=1}^M |d_i - \hat{d}_i|/d_i$ , (2)

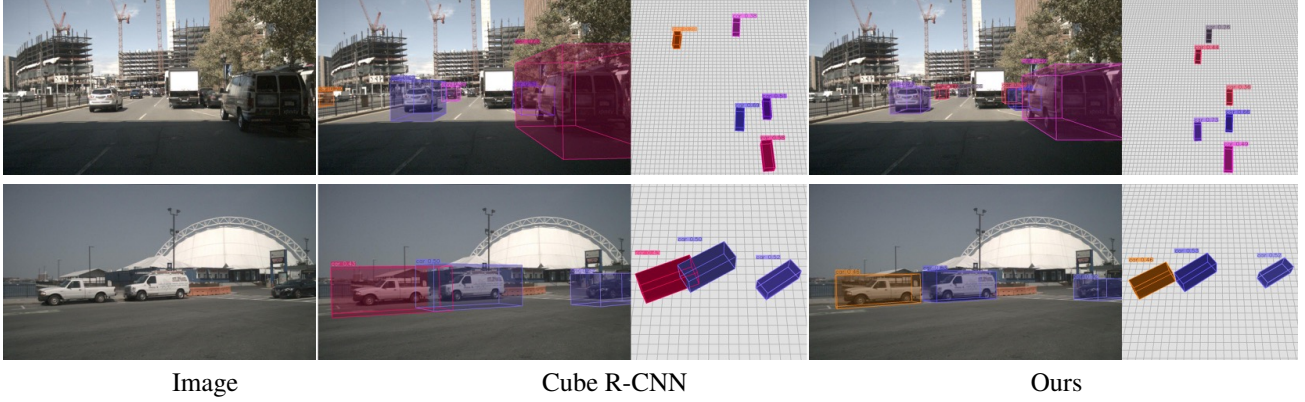


Figure 7. **3D Object Detection on nuScenes.** We show the 3D bounding box predictions on Cars category for Cube R-CNN [6] and our model (Cube R-CNN + KPE), both in image space and in top-down view. Our model performs better, as evident by fewer collisions (*i.e.* intersections between car bounding boxes) and missed detections. More visualizations on KITTI and nuScenes in supplementary.

**RMSE:** root mean squared error,  $[\frac{1}{M} \sum_{i=1}^M |d_i - \hat{d}_i|^2]^{\frac{1}{2}}$ , (3)  
 $\log_{10}$ : average  $\log_{10}$  error,  $\frac{1}{M} \sum_{i=1}^M |\log_{10} d_i - \log_{10} \hat{d}_i|$ .

**Results:** From the results in Tab. 2, we observe that training and evaluating the model at lower resolution crops leads to a considerable drop in performance, even when using the MiDaS initialization. This is expected, as pointed out in several works [6, 29, 39], due to the drawbacks of using cropping and scaling augmentations in these models during training. Next, we consider the impact of adding KPE. We observe larger gains in the lower resolution  $96 \times 128$  setting with augmentations, indicating that our encoding is indeed useful. We observe little improvement at the  $384 \times 512$  resolution, which is likely due to the strong initialization provided by the large MiDaS model which is pre-trained on 12 different datasets at the same resolution.

In terms of design choices, we see gains when adding KPE to the downsampled image features before it is passed to the BeiT [2] module. This allows the transformer to incorporate information about the crop location in the camera’s field of view in the multi-scale feature output. We find that adding KPE to the features from the MiDaS backbone along with the predicted relative depth is not very effective. This could be because most of the capacity of the model lies in the MiDaS backbone (327M+ parameters) and the domain-specific decoder at the end may not need additional cues for refining the depth. From Tab. 4, we find the dense variant of the encoding to work better than the sparse variant. This is likely due to the dense prediction nature of this task.

In Fig. 6, we visualize the predicted depth along with the squared error  $\Delta$  w.r.t. to ground truth (ranging from dark blue: low to dark red: high). Our model predicts better depth as evident by lower  $\Delta$  (lower intensity red areas). More visualizations are provided in supplementary.

Method	AP <sub>3D</sub> <sup>25</sup> ↑	AP <sub>3D</sub> <sup>50</sup> ↑	AP <sub>3D</sub> <sup>75</sup> ↑	AP <sub>3D</sub> ↑
<b>KITTI Dataset</b>				
Cube R-CNN	72.59	44.80	14.68	56.11
Cube R-CNN + KPE	<b>73.02</b>	<b>47.08</b>	<b>16.34</b>	<b>57.50</b>
<b>nuScenes Dataset</b>				
Cube R-CNN	72.83	50.45	<b>18.76</b>	58.53
Cube R-CNN + KPE	<b>74.03</b>	<b>51.50</b>	18.27	<b>59.48</b>
<b>KITTI + nuScenes</b>				
Cube R-CNN	70.17	43.83	14.23	54.59
Cube R-CNN + KPE	<b>73.10</b>	<b>47.51</b>	<b>16.58</b>	<b>57.54</b>

Table 3. **3D Object Detection results.** We add KPE to the Cube R-CNN [6] model and compare the AP scores at different IoUs. We see consistent improvements across all metrics in both single dataset and joint dataset training. The gains are more prominent in the mutli-dataset setting since we incorporate camera intrinsic information in KPE. We use the sparse KPE variant here.

### 5.3. 3D Object Detection on KITTI and nuScenes

**Task:** The goal is to predict the 3D bounding box of objects from a single image. Several methods [6, 18, 30] on this task involve predicting 2D bounding box proposals from the features extracted using a backbone, followed by a decoder which uses the features corresponding to the pixels in the box proposal to regress to the 3D bounding box. We investigate whether KPE can augment the box features with additional cues to aid with the 3D regression.

**Method:** We use the recent Cube R-CNN [6] model since it provides a generic framework for 3D detection, without any domain or object specific strategies. It consists of a convolutional backbone to extract features from an image, followed by a region proposal network [30] to predict regions of interest (RoIs) (represented as 2D box proposals) used for



	KITTI			NYU			ARCTIC		
	AP <sub>3D</sub> <sup>50</sup> ↑	AP <sub>3D</sub> <sup>70</sup> ↑	AP <sub>3D</sub> ↑	REL ↓	RMSE ↓	log <sub>10</sub> ↓	AAE ↓	CDev ↓	Acc ↓
KPE sparse	<b>47.08</b>	<b>16.34</b>	<b>57.50</b>	0.097	0.388	0.041	<b>5.92</b>	39.39	<b>8.72</b>
KPE dense	45.11	15.16	55.96	<b>0.088</b>	<b>0.353</b>	<b>0.038</b>	6.16	<b>37.71</b>	9.36

Table 4. **Ablation on KPE.** We compare two variants of KPE: sparse and dense (Sec. 4). We observe that sparse encoding is better for sparse prediction tasks and dense encoding is better for dense prediction tasks.

detecting objects. The features from each detected object are passed to a decoder to predict a 3D bounding box. The model is trained using 3D ground truth supervision for the 3D bounding box on multiple datasets jointly. Since each of these datasets are collected using different cameras, the authors propose to augment camera information with the ground truth depth used for training. This is referred to as virtual depth [6] and is orthogonal to our proposed KPE encoding. Please refer to [6] for more details.

**Modifications:** We use the same training protocol as [6].

**Incorporating KPE:** The region proposal network in the backbone predicts 2D box proposals which are used for detecting objects. The positive box proposals with detected objects are then passed to the cube head to regress the 3D bounding box. We incorporate KPE along with the features of the positive 2D box proposals before feeding to the cube head for 3D regression. Similar to Sec. 5.1 and Sec. 5.2, we explore both the sparse and the dense variant of our encoding. For the sparse variant, we broadcast the features to match the feature resolution whereas for the dense variant, we interpolate the features to the desired feature resolution.

**Dataset:** We experiment on two commonly used datasets in 3D detection: KITTI [13] and nuScenes [7]. We select these datasets since they capture urban outdoor scenes with a wide field of view, a setting in which perspective distortion is more prominent. We use the same splits as [6]: (1) KITTI: 2.8K training images & 329 validation images, (2) nuScenes: 18K training & 1.1K validation images, and focus on the Cars category. We consider two settings: (1) single dataset training on KITTI and nuScenes separately, (2) joint dataset training on both KITTI and nuScenes. Since KPE contains camera information, we hypothesize that it should be effective in joint dataset training as well. In the joint training on KITTI and nuScenes, we compare with the Cube-RCNN variant that does not use virtual depth to disentangle the impact of virtual depth in multi-camera setting.

**Metrics:** Following prior work [6], we utilize average-precision (AP) as our metric to evaluate the 3D object detection models. The predicted 3D cuboid is matched to the ground truth 3D cuboid by computing a 3D intersection-over-union (IoU). We also report the AP over a range of different IoU thresholds.

**Results:** We observe consistent improvements in AP at different IoU thresholds in both the single dataset and the joint dataset settings in Tab. 3. The gains are more prominent in the multi-dataset setting since we incorporate camera intrinsic information into our KPE encoding. From the ablation in Tab. 4, we see that the sparse variant performs better than the dense variant. This is similar to the 3D pose estimation results in Sec. 5.1, which may be due to the fact that both of these tasks involve making a sparse 3D prediction, unlike the depth estimation model in Sec. 5.2.

We also visualize the 3D bounding box predictions on Cars category for Cube R-CNN [6] & our model (Cube R-CNN + KPE) in Fig. 7, both in image space & in top-down view. Our model performs better, as evident by fewer collisions (*i.e.* intersections between car bounding boxes) and missed detections. More visualizations on KITTI & nuScenes are in supplementary.

## 6. Conclusion

We explore the ambiguity induced by perspective distortion in image crops. We provide an intuitive understanding of this ambiguity using parallelepipeds and propose an intrinsics-aware positional encoding (KPE) that incorporates the location of the image crop in the field of the view of the camera. KPE is effective on several tasks involving prediction of 3D attributes from a single image, *i.e.* 3D pose estimation of articulated objects in contact, dense metric depth prediction, and 3D object detection. As future work, we could apply KPE to tasks involving the prediction of fine-grained attributes, *e.g.* full 3D shape from a single image.

**Limitations:** Our analysis only considered geometry of projection. It will be interesting to assess if shading or other cues help alleviate the ambiguity. Our KPE encoding requires camera intrinsics which are typically present in image metadata but they may not always be available.

**Acknowledgements:** We thank Matthew Chang, Shaowei Liu, Anand Bhattad & Kashyap Chitta for feedback on the draft, and David Forsyth for useful discussion. This material is based upon work supported by an NSF CAREER Award (IIS2143873), NASA (80NSSC21K1030), an NVIDIA Academic Hardware Grant, and the NCSA Delta System (supported by NSF OCI 2005572 and the State of Illinois).



## References

- [1] Manuel Lopez Antequera, Pau Gargallo, Markus Hofinger, Samuel Rota Buló, Yubin Kuang, and Peter Kontschieder. Mapillary planet-scale depth dataset. In *ECCV*, 2020. 2
- [2] Hangbo Bao, Li Dong, Songhao Piao, and Furu Wei. BEiT: BERT pre-training of image transformers. In *ICLR*, 2022. 6, 7
- [3] Shariq Farooq Bhat, Ibraheem Alhashim, and Peter Wonka. Localbins: Improving depth estimation by learning local distributions. In *ECCV*, 2022. 6
- [4] Shariq Farooq Bhat, Reiner Birkel, Diana Wofk, Peter Wonka, and Matthias Müller. Zoedepth: Zero-shot transfer by combining relative and metric depth. *arXiv*, 2023. 2, 6
- [5] Adnane Boukhayma, Rodrigo Andrade de Bem, and Philip H. S. Torr. 3d hand shape and pose from images in the wild. In *CVPR*, 2019. 4
- [6] Garrick Brazil, Abhinav Kumar, Julian Straub, Nikhila Ravi, Justin Johnson, and Georgia Gkioxari. Omni3d: A large benchmark and model for 3d object detection in the wild. In *CVPR*, pages 13154–13164, 2023. 2, 7, 8
- [7] Holger Caesar, Varun Bankiti, Alex H. Lang, Sourabh Vora, Venice Erin Liong, Qiang Xu, Anush Krishnan, Yu Pan, Giancarlo Baldan, and Oscar Beijbom. nuscenes: A multimodal dataset for autonomous driving. In *CVPR*, 2020. 2, 8
- [8] Alexey Dosovitskiy, Lucas Beyer, Alexander Kolesnikov, Dirk Weissenborn, Xiaohua Zhai, Thomas Unterthiner, Mostafa Dehghani, Matthias Minderer, Georg Heigold, Sylvain Gelly, et al. An image is worth 16x16 words: Transformers for image recognition at scale. In *ICLR*, 2021. 2
- [9] David Eigen, Christian Puhrsch, and Rob Fergus. Depth map prediction from a single image using a multi-scale deep network. *NeurIPS*, 27, 2014. 2, 6
- [10] William Epstein. The known-size-apparent-distance hypothesis. *The American journal of psychology*, 74(3):333–346, 1961. 1
- [11] Jose M Facil, Benjamin Ummenhofer, Huizhong Zhou, Luis Montesano, Thomas Brox, and Javier Civera. Cam-convs: Camera-aware multi-scale convolutions for single-view depth. In *CVPR*, pages 11826–11835, 2019. 2
- [12] Zicong Fan, Omid Taheri, Dimitrios Tzionas, Muhammed Kocabas, Manuel Kaufmann, Michael J. Black, and Otmar Hilliges. ARCTIC: A dataset for dexterous bimanual hand-object manipulation. In *CVPR*, 2023. 2, 4, 5
- [13] Andreas Geiger, Philip Lenz, and Raquel Urtasun. Are we ready for autonomous driving? the kitti vision benchmark suite. In *CVPR*, 2012. 2, 8
- [14] Vitor Guizilini, Igor Vasiljevic, Jiading Fang, Rare Ambru, Greg Shakhnarovich, Matthew R Walter, and Adrien Gaidon. Depth field networks for generalizable multi-view scene representation. In *ECCV*, 2022. 2
- [15] Vitor Guizilini, Igor Vasiljevic, Dian Chen, Rare Ambruş, and Adrien Gaidon. Towards zero-shot scale-aware monocular depth estimation. In *ICCV*, 2023. 2
- [16] Shreyas Hampali, Sayan Deb Sarkar, Mahdi Rad, and Vincent Lepetit. Keypoint transformer: Solving joint identification in challenging hands and object interactions for accurate 3d pose estimation. In *CVPR*, 2022. 5
- [17] Kaiming He, Xiangyu Zhang, Shaoqing Ren, and Jian Sun. Deep residual learning for image recognition. In *CVPR*, 2016. 4
- [18] Kaiming He, Georgia Gkioxari, Piotr Dollár, and Ross B. Girshick. Mask R-CNN. In *ICCV*, 2017. 4, 7
- [19] William H Ittelson. Size as a cue to distance: Static localization. *The American journal of psychology*, 64(1):54–67, 1951. 1
- [20] Linyi Jin, Jianming Zhang, Yannick Hold-Geoffroy, Oliver Wang, Kevin Blackburn-Matzen, Matthew Sticha, and David F Fouhey. Perspective fields for single image camera calibration. In *CVPR*, pages 17307–17316, 2023. 2
- [21] Angjoo Kanazawa, Michael J. Black, David W. Jacobs, and Jitendra Malik. End-to-end recovery of human shape and pose. In *CVPR*, 2018. 2
- [22] Angjoo Kanazawa, Shubham Tulsiani, Alexei A Efros, and Jitendra Malik. Learning category-specific mesh reconstruction from image collections. In *ECCV*, 2018. 4
- [23] Abhishek Kar, Shubham Tulsiani, Joao Carreira, and Jitendra Malik. Amodal completion and size constancy in natural scenes. In *ICCV*, pages 127–135, 2015. 2
- [24] Muhammed Kocabas, Chun-Hao P. Huang, Otmar Hilliges, and Michael J. Black. PARE: part attention regressor for 3d human body estimation. In *ICCV*, 2021. 4
- [25] Rosanne Liu, Joel Lehman, Piero Molino, Felipe Petroski Such, Eric Frank, Alex Sergeev, and Jason Yosinski. An intriguing failing of convolutional neural networks and the coordconv solution. *NeurIPS*, 31, 2018. 2
- [26] Jitendra Malik and Ruth Rosenholtz. Computing local surface orientation and shape from texture for curved surfaces. *IJCV*, 1997. 2
- [27] Takeru Miyato, Bernhard Jaeger, Max Welling, and Andreas Geiger. GTA: A geometry-aware attention mechanism for multi-view transformers. *arXiv*, 2023. 2
- [28] Rene Ranftl, Alexey Bochkovskiy, and Vladlen Koltun. Vision transformers for dense prediction. In *ICCV*, 2021. 6
- [29] René Ranftl, Katrin Lasinger, David Hafner, Konrad Schindler, and Vladlen Koltun. Towards robust monocular depth estimation: Mixing datasets for zero-shot cross-dataset transfer. *TPAMI*, 44(3), 2022. 2, 6, 7
- [30] Shaoqing Ren, Kaiming He, Ross Girshick, and Jian Sun. Faster r-cnn: Towards real-time object detection with region proposal networks. In *NeurIPS*, 2015. 7
- [31] Nathan Silberman, Derek Hoiem, Pushmeet Kohli, and Rob Fergus. Indoor segmentation and support inference from rgb-d images. In *ECCV*, pages 746–760. Springer, 2012. 2, 6
- [32] Jianlin Su, Yu Lu, Shengfeng Pan, Bo Wen, and Yunfeng Liu. Roformer: Enhanced transformer with rotary position embedding. *arXiv*, 2021. 2
- [33] Yutao Sun, Li Dong, Barun Patra, Shuming Ma, Shaohan Huang, Alon Benhaim, Vishrav Chaudhary, Xia Song, and Furu Wei. A length-extrapolatable transformer. In *ACL*, 2022. 2
- [34] Omid Taheri, Nima Ghorbani, Michael J Black, and Dimitrios Tzionas. GRAB: A dataset of whole-body human grasping of objects. In *ECCV*, 2020. 5

- [35] Ashish Vaswani, Noam M. Shazeer, Niki Parmar, Jakob Uszkoreit, Llion Jones, Aidan N. Gomez, Lukasz Kaiser, and Illia Polosukhin. Attention is all you need. *NeurIPS*, 2017. [2](#)
- [36] Leonardo Da Vinci. A treatise on painting, 1632. [1](#)
- [37] Wang Yifan, Carl Doersch, Relja Arandjelović, Joao Carreira, and Andrew Zisserman. Input-level inductive biases for 3d reconstruction. In *CVPR*, 2022. [2](#)
- [38] Xiong Zhang, Qiang Li, Hong Mo, Wenbo Zhang, and Wen Zheng. End-to-end hand mesh recovery from a monocular rgb image. In *ICCV*, 2019. [4](#)
- [39] Yuanyi Zhong, Anand Bhattad, Yu-Xiong Wang, and David Forsyth. Improving equivariance in state-of-the-art supervised depth and normal predictors. In *ICCV*, 2023. [6](#), [7](#)